

We are IntechOpen, the world's leading publisher of Open Access books Built by scientists, for scientists

6,900

Open access books available

186,000

International authors and editors

200M

Downloads

Our authors are among the

154

Countries delivered to

TOP 1%

most cited scientists

12.2%

Contributors from top 500 universities



WEB OF SCIENCE™

Selection of our books indexed in the Book Citation Index
in Web of Science™ Core Collection (BKCI)

Interested in publishing with us?
Contact book.department@intechopen.com

Numbers displayed above are based on latest data collected.
For more information visit www.intechopen.com



Quantum Information Science in High Energy Physics

Oliver Keith Baker

Abstract

We demonstrate that several anomalies seen in data from high energy physics experiments have their origin in quantum entanglement, and quantum information science more generally. A few examples are provided that help clarify this proposition. Our research clearly shows that there is a thermal behavior in particle kinematics from high energy collisions at both collider and fixed target experiments that can be attributed to quantum entanglement and entanglement entropy. And in those cases where no quantum entanglement is expected, the thermal component in the kinematics is absent, in agreement with our hypothesis. We show evidence that these phenomena are interaction independent, but process dependent, using results from proton-proton scattering at the Large Hadron Collider (LHC) and antineutrino-nucleus scattering at Fermilab. That is, this thermal behavior due to quantum entanglement is shown to exist in both the strong and electroweak interactions. However, the process itself must include quantum entanglement in the corresponding wave functions of interacting systems in order for there to be thermalization.

Keywords: Quantum Entanglement, Entanglement Entropy, High Energy Physics

1. Introduction

A complete understanding of multi-particle production dynamics continues to be a challenge for theory in high energy collisions. The full description of real-time dynamical evolution in a strongly coupled non-Abelian gauge theory can be notoriously difficult. The availability of large, diverse, and high quality accumulated proton-proton (pp) and heavy ion (HI) collision data from the energy frontier at the Large Hadron Collider (LHC) and at Brookhaven National Laboratory's Relativistic Heavy Ion Collider (RHIC) are providing new insights into puzzling behavior observed in these strong interaction processes. Additionally, studies of similar intensity frontier anomalies in (anti)neutrino-nucleus scattering gathered recently also benefit from newly accumulated event statistics at Fermilab. The transverse momentum distribution of differential cross sections in pp collisions shows process-dependent behavior that requires a more subtle explanation compared to previous ideas.

For example, the differential distribution of charged hadrons resulting from pp collisions are observed to exhibit both a well-understood quark and gluon "hard scattering" component at high transverse momenta that can best be described by a power-law fit to the distribution, and a component at low transverse momenta that

exhibits a less well-understood “thermal” behavior that is best represented by an exponential fit to the data [1, 2]. See [3, 4] for a review. The sum of these two contributions is necessary to properly characterize the transverse momentum differential distribution. And yet, for diffractive events where there is a large rapidity gap in the transverse momentum distribution of the differential cross section for photo-produced muon pairs, there is only a hard-scattering contribution; the thermal component disappears in this class of processes even though these inelastic events produce large number of hadrons. Charged-current weak interactions also exhibit differential cross section momentum distributions that have process-dependent results. As in the case of strong interactions, for anti-neutrino scattering from a nucleon inside a nucleus, there is also a “hard scattering” component at high particle momenta that is manifested by a power-law fit to the momentum distribution of the differential cross section. And at low momenta, the differential cross section behavior is best described by an exponential fit to the momentum distribution in this region. Furthermore, in coherent anti-neutrino scattering from a nucleus, where the nucleus remains intact, there is no thermal component to the differential cross section momentum distribution, only the hard-scattering component [5].

It is interesting to consider the possibility that these two interactions of vastly differing collision or scattering energies are different manifestations of a single underlying fundamental process. There is growing interest in the link between quantum entanglement, entanglement entropy (EE), and high energy physics presently. Here, we describe a relationship between quantum entanglement in the nucleon wave functions associated with the hadron collisions at the LHC experiments and with the electroweak scattering in Fermilab experiments. There are several examples of these relationships in theoretical physics: Research on the dynamics of quantum entanglement and entanglement entropy in the regime of small Bjorken- x in deep inelastic scattering, in electromagnetic interactions [6]. Additionally in [1] the case is made that quantum entanglement between partons inside a nucleon can be probed by deep inelastic lepton scattering. Deeper insights into these dynamics involving entanglement entropy in the regions of black holes is now provided by the AdS/CFT correspondence [7]. Well-understood quark-antiquark correlations are now improved even more due to considerations of entanglement entropy in Lattice Gauge Theory [8] that are or soon will be augmented by new and planned parton distribution functions data in particle and nuclear physics. Newer intuition into this relationship that involves quantum entanglement, entanglement entropy, thermal behavior, is gained from heavy ion and proton-proton collisions [9, 10], nuclear shadowing effects [11], and chiral symmetry breaking [12].

In [1, 2, 13], it is proposed that the thermal component is a result of entanglement between causally disconnected parts of the nucleon in the interaction. For this reason inelastic pp collisions exhibit a thermal component, while diffractive collisions, where the nucleon as a whole is probed, give rise to only the hard-scattering component, and no thermal behavior. That the thermal component is a consequence of quantum entanglement between different regions of the colliding protons wave functions in pp collisions is proposed in [14]. A thermal behavior can, in the collisions where there are large number of particle produced in the final state, be the result of rescattering among the produced final state particles. However, the thermal component was shown to not only be present in the transverse momentum distribution of charged hadrons, but also in the transverse momentum spectrum of Higgs bosons production and decay differential cross section, resulting from the collisions. For Higgs boson production in pp collisions, there are very few final state particles for rescattering compared to heavy ion collisions for example.

If quantum entanglement and EE are responsible for the thermal behavior in charged hadron as well as Higgs boson production in pp collisions at the LHC, then it should also be observed in neutrino-nucleus scattering, where only a fraction of the struck nucleon in the interaction is probed by the exchanged charged-current probe. As explained in [5] the observation of a thermal component exists in the momentum distribution of neutral pions from antineutrino-nucleon scattering, while no such component is present in coherent antineutrino-nucleon scattering. This absence of a thermal component in the latter case is due to the fact that antineutrinos probe the nucleus as a whole in coherent scattering; there is no un-probed region of the nucleus which can be entangled with the probed region. So with no quantum entanglement in the interaction, the thermal component in the momentum distribution of the differential cross section is absent, as expected.

These topics are presented and discussed in this chapter. A brief description of the theory motivating this proposed link between quantum entanglement, entanglement entropy, and thermal behavior in pp collisions is given in Section 2 and subSection 2.1. This is followed by experimental results of transverse momentum distributions in pp collisions at 13 TeV collisions energy. Charged hadron production where (and why) both hard scattering and thermal components are present in the differential distribution are described in subSection 2.2. The absence of the thermal component in diffractive production of muon pairs in the reaction $pp \rightarrow \mu^+ \mu^- X$ is explained in subSection 2.3. The interesting need for superposition of both the hard scattering and thermal components to describe the transverse momentum distribution of the Higgs boson is presented in subSection 2.4. Section 3 includes the presentation of this phenomena in charged current weak interactions. Concluding remarks are given in Section 4.

2. Entanglement entropy and thermal behavior in the strong interaction

We begin by considering the possibility that the observed thermalization in pp collisions is the result of a sudden perturbation or rapid “quench” due to the high degree of entanglement inside the protons involved in the collision [15]. The link between quantum thermalization and quantum entanglement is shown to exist in an experimental quench in Bose-Einstein condensates of Rb atoms in atomic and condensed matter physics [16]; the rapid eigenstate thermalization was found to be the result of a quantum entanglement. In pp process described here, low momenta correspond to late times after the collision. The thermal behavior begins to dominate over the hard scattering component in the transverse momentum distribution at late times. This is consistent with theoretical studies in $(1 + 1)$ -dimensional conformal field theories of quenches in entangled quantum systems [17–19] where a system can be described by a generalized thermal Gibbs ensemble at late times.

Since a high-energy collision can be viewed as a rapid quench of the entangled partonic state [15], it is thus possible that the effective temperature inferred from the transverse momentum distributions of the secondaries in a collision can depend upon the momentum transfer, that is an ultraviolet cutoff on the quantum modes resolved by the collision. In analyzing the high-energy collisions with different characteristic momentum transfer Q we thus expect to find different effective temperatures $T \sim Q$. We can also look at the inelastic events characterized by a rapidity gap, where the proton is probed as a whole, and no entanglement entropy arises [15]. In this case, if the quantum entanglement is responsible for the thermalization, we expect no thermal radiation.

The presence of both a thermal and a hard scattering component in inclusive deep-inelastic scattering at HERA has been observed [20]. And the absence of this thermal component in processes characterized by a rapidity gap is also manifested in these studies. In diffractive events where there is a rapidity gap, the entire proton wave function is involved in the scattering process. In diffractive scattering, the proton remains fully intact in the central part of the collider detector where scattering takes place. There is no entanglement entropy due to different regions of the proton wave function being involved in the scattering in different ways. This observation points to a connection between this thermalization and quantum entanglement between different parts of the proton wave function. This link is described in the next section.

2.1 Entanglement and thermalization in high energy collisions - theory

A brief summary of these proposition is as follows. The hard process in pp collisions probes only the part of the proton wave function that is localized in a region of space denoted here as **A**. For a hard process such as the one shown in **Figure 1** this region has a transverse size that is less than the full proton diameter and, in the proton's rest frame, longitudinal size in terms of Bjorken- x is $\sim (mx)^{-1}$, where m is the proton mass.

In this same figure, the spatial region **B** is complementary to **A**, that is, the entire space is **A** \cup **B**. Hard processes have their origin in the physical states inside the region **A**. These are states in a Hilbert space \mathcal{H}_A of dimension n_A . Unobserved states (not part of hard scattering) in the region **B** belong to the Hilbert space \mathcal{H}_B of dimension n_B . With this picture, the protons prior to the collision, both composite systems in **A** \cup **B** (the entire proton in each case) are then separately described by the vector represented as, for example, $|\psi_{AB}\rangle$ in a tensor product of the two spaces $\mathcal{H}_A \otimes \mathcal{H}_B$:

$$|\psi_{AB}\rangle = \sum_{i,j} c_{ij} |\varphi_i^A\rangle \otimes |\varphi_j^B\rangle, \quad (1)$$

where c_{ij} are the elements of the matrix C that has a dimension $n_A \times n_B$. In the case where there are states $|\varphi^A\rangle$ and $|\varphi^B\rangle$ that $|\psi_{AB}\rangle = |\varphi^A\rangle \otimes |\varphi^B\rangle$, where that the sum (Eq. (1)) contains only one term, then the state $|\psi_{AB}\rangle$ is product state that is separable. In the case where it is not separable, $|\psi_{AB}\rangle$ is entangled.

$|\psi_{AB}\rangle$ is called a bi-partite system that, making use of the Schmidt decomposition theorem, can be expanded as a *single* sum in n instead of a double sum over ij .

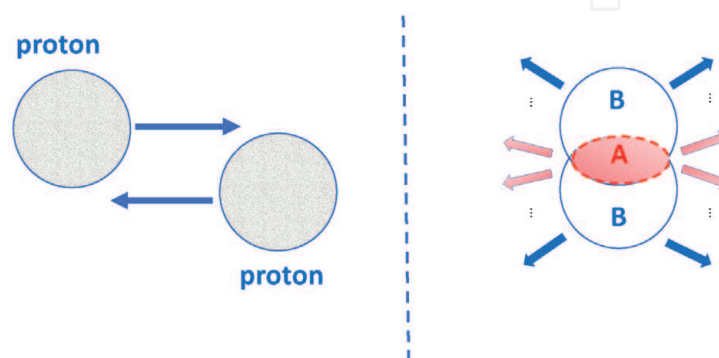


Figure 1.

Characterization of the entanglement entropy in pp collisions. In the leftmost depiction, the collider protons, before collision, are both pure states. In the rightmost depiction, during the pp scattering, there exists the proton overlap collision region (**A**) and the overlap spectator region (**B**).

$$|\psi_{AB}\rangle = \sum_n \alpha_n |\psi_n^A\rangle |\psi_n^B\rangle \quad (2)$$

Here $|\psi_n^A\rangle$ and $|\psi_n^B\rangle$ are orthonormal sets of states (properly chosen) localized in the domains **A** and **B**, respectively. And α_n are real, positive numbers that are the square roots of the eigenvalues of matrix CC^\dagger .

The density matrix formalism is now a better tool to use in the discussion. For a mixed state that is probed in region *A*, the density matrix can be expressed as

$$\rho_A = \text{tr}_B \rho_{AB} = \sum_n \alpha_n^2 |\psi_n^A\rangle \langle \psi_n^A|, \quad (3)$$

where the symbol $\alpha_n^2 \equiv p_n$ denotes the probability of an *n*-parton state. The basis $|\psi_n^A\rangle$ in (Eq. (2)) with states having a fixed number of *n* partons does not have interference between states with different number of partons due to the fact that this sort of interference is absent in the parton model. In this Schmidt decomposition, there can be an infinite number of terms (the Schmidt rank) in the sum shown in (Eq. (2)). A Schmidt rank one state is then a pure product state that does not include entanglement.

In the case of a mixed state, the probabilities corresponding to the different states described above can be used to define the von Neumann entropy of the mixed state given by

$$S = -\sum_n p_n \ln p_n. \quad (4)$$

It is the entanglement between regions **A** and **B** defined above that gives rise to what is called entanglement entropy here, and is related to Shannon entropy in information theory shown in (Eq. (4)). Hence the entanglement entropy can be determined from the QCD evolution equations that are used to evaluate the probabilities p_n . After the hard scattering takes place in the collision, the mixed quantum state characterized by the entanglement entropy (Eq. (4)) undergoes the evolution towards the final asymptotic state of hadrons that are measured by the detectors. This final state is characterized by the Boltzmann entropy. Further discussions of the relationship between Boltzmann entropy and entanglement entropy can be found in [14].

Studies of quantum entanglement and thermalization in atomic and condensed matter physics were shown to depend upon the quench properties, and that there is evidence for quantum propagation and information propagation [16, 21–23]. It is instructive to compare this with a quench induced by a high energy collision. The quench associated with the latter [17, 18] leads to the following interpretation. A quench produces a highly excited state of a Hamiltonian $H = H_0 + V(t)$ from what was the ground state of an unperturbed Hamiltonian H_0 originally. Here $V(t)$ is the term induced by the inelastic collision. Gluon exchange in the strong interaction induces the inelastic interaction, so the term $V(t)$ is seen to represent an effect of the pulse of the color field. The onset of this pulse in a hard scattering with a hardness scale Q , by the uncertainty principle, is $\tau \sim 1/Q$ where τ is the proper time. Since this time is short on the QCD scale, $\tau \ll 1/\Lambda$, the quench creates a highly excited multi-particle state. A short pulse of (chromo)electric field produces particles that have a thermal-like exponential spectra. The thermal spectrum in this case can be attributed to the emergence of an event horizon formed due to the acceleration induced by the electric field. Associated with this system is an effective temperature of $T \simeq (2\pi\tau)^{-1} \simeq Q/(2\pi)$ [24–27].

As shown in [17, 18] for a rapid quench (such as the one that occurs in a high-energy collision) in a $(1 + 1)$ dimensional CFT the entanglement entropy of a segment of length L first grows linearly in time, until $t \simeq L/2$, and then saturates at the value

$$S(t) \simeq \frac{c}{3} \ln \tau_0 + \frac{\pi c L}{12 \tau_0}. \quad (5)$$

where c is the conformal charge of the CFT, and τ_0^{-1} is the energy cutoff for the ultraviolet modes [14]. A sketch of the picture of the resulting thermalization from entanglement caused by the quench is shown in **Figure 2**.

The interpretation of the result (5) is the following [17, 18]. The quench leads to the production of entangled (quasi)particle pairs, since what used to be the ground state of the undisturbed Hamiltonian H_0 is a highly excited state of the Hamiltonian after the quench, $H = H_0 + V(t)$. The entangled pairs produced by the quench propagate along the light cone, and contribute to the entanglement entropy of the segment of length L if only one particle of the pair is detected within this segment. Shortly after the quench, only particle pairs produced near the boundary of the segment thus contribute to the entanglement, and the entanglement entropy is not extensive in the length L . However, at times $t > L/2$, even in the center of the segment one can detect a particle whose entangled partner is outside of the segment – this means that the entanglement entropy receives contributions from the entire segment, and should scale extensively in L in accord with the result (5). This scaling is a necessary condition for an effective thermalization.

For a quench induced by a high-energy collision, we sketch the resulting picture of thermalization from entanglement in **Figure 2**. Note that the hardest quasiparticle modes that propagate along the light cone thermalize first. For the softer

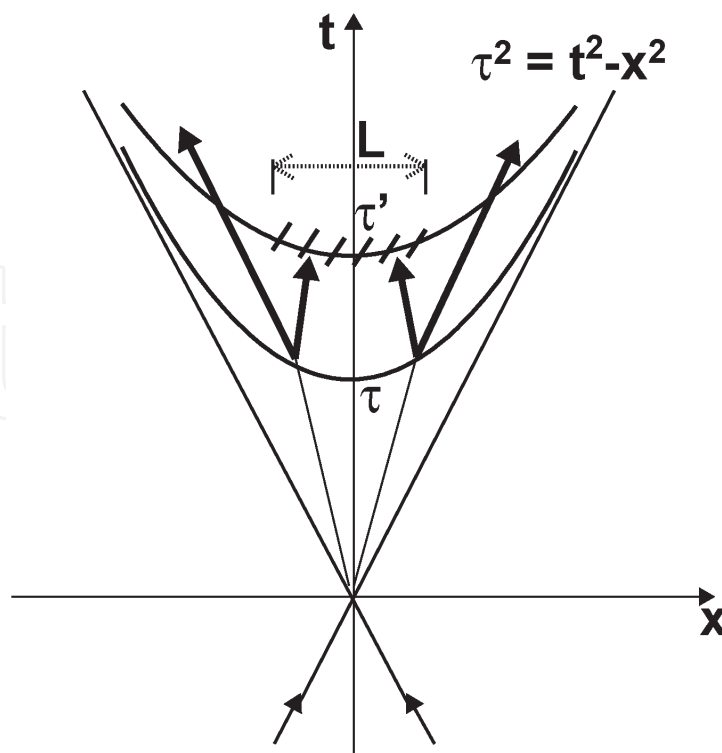


Figure 2.

An illustration of the onset of quantum thermalization through entanglement in a high energy pp collision. Time runs along the vertical axis, while space runs along the horizontal axis. The outermost lines define the light cone. The variables used are defined in the text. Entangled particle pairs that are produced at a proper time $\tau < \tau'$ contribute to the entanglement entropy in the interval of length L shown by the hashed segment of the curve. Figure from [14].

particles that propagate in the interior of the light cone, it takes a longer time to thermalize, that is, to exhibit an extensive scaling of the entropy. The detection of particles is assumed to be performed within the interval of length L (see Eq. (5)), corresponding to a limited range in (pseudo)rapidity. While (Eq. (5)) has been obtained in the framework of CFT, the simple physical interpretation of this result makes its broader validity quite likely.

It is instructive to point out the difference in the mechanisms of thermalization expected at weak and strong coupling. At weak coupling, the “bottom-up” thermalization mechanism [28] also yields an effective temperature $T \sim Q_s$ in inelastic high energy collisions. However the thermalization in this picture begins from the soft, low-momentum modes that eventually draw the energy from the harder modes; the thermalization of the hard, high-momentum modes is thus expected to take a parametrically long time proportional to the inverse power of the (small) coupling constant [28]. On the other hand, in strongly coupled entangled systems the process of thermalization is fast and determined by the size of the system and the parameters of the quench; moreover, it starts from the *hardest* modes resolved in the process. In the dual holographic description of conformal field theory, this process is described by the formation of trapped surface near the Minkowski boundary that then falls into the AdS bulk, corresponding to the spreading of thermalization from hard to soft modes [29, 30]. A similar picture emerges from the analysis of entanglement entropy in an expanding string [31], where the entropy has been found to have a thermal form with an effective temperature $T \sim 1/\tau$ at early time τ .

2.2 Charged hadron transverse momentum distribution

The discussion presented in the previous sections provide motivation to compare with experimental results from inelastic collision events at high energies. It also gives the opportunity to explore the possible relation between effective temperature and the hard scale of the collision. Consider proton-proton collisions data recorded by the LHC ATLAS collaboration at $\sqrt{s} = 13$ TeV center of mass energy yield multiple charged particles in the final state [32]. The data presented here corresponds to $151 \mu\text{b}^{-1}$ of integrated luminosity for charged particles with greater than 100 MeV/c transverse momenta and absolute pseudorapidity of less than 2.5. Events with two or more final state charged particles were selected in the analysis. Final state hadrons that originate in the primary pp interaction and that have a lifetime of greater than 30 ps were excluded from the final selected events in order to remove the presence of charged particles that have strangeness or are from heavier flavors.

The normalized charged hadron transverse momentum distribution is shown in **Figure 3**. The thermal component is shown by the exponential, red dashed curve; we parameterize it as

$$\frac{1}{p_T} \frac{d^2 N_{ev}}{dp_T} = A_{therm} \exp(-m_T/T_{th}), \quad (6)$$

where m_T , the hadron transverse mass, is defined as by $m_T \equiv \sqrt{m^2 + p_T^2}$ (m is the hadron mass; dominated by pions it is assumed), and T_{th} is an effective temperature. The hard scattering (power law, green solid curve) component is parameterized similar to [13],

$$\frac{1}{p_T} \frac{d^2 N_{ev}}{dp_T} = \frac{A_{hard}}{\left(1 + \frac{m_T^2}{T^2 n}\right)^n}, \quad (7)$$

where T and n are parameters to be determined from the fit. The sum of the thermal and hard scattering contribution terms is shown by the blue solid curve in **Figure 3**.

The extracted value of the thermal temperature, $T_{th} = 0.17$ GeV describes well the experimental transverse momentum distribution, and it agrees with the temperature expected from the extrapolation of the relation [13] deduced at lower energies;

$$T_{th} = 0.098 \cdot \left(\sqrt{s/s_0} \right)^{0.06} \text{ GeV} \quad (8)$$

to the LHC 13 TeV collision energy; here $s_0 = 1 \text{ GeV}^2$. Similarly, the hard scale temperature parameter T is [13]

$$T = 0.409 \cdot \left(\sqrt{s/s_0} \right)^{0.06} \text{ GeV}. \quad (9)$$

It's interesting that the parameterizations (Eqs. (8) and (9)) imply that the effective thermal temperature T_{th} is proportional to the hard scale temperature parameter T , which is in agreement with the Section 2.1 discussion.

The fits to the charged hadron transverse momentum distribution in **Figure 3** yields the hard scale temperature parameter $T = 0.72$ GeV and $n = 3.1$, in agreement with the extrapolation of (Eq. (9)) to 13 TeV pp collision energy, but with a smaller value of n . This reflecting the slower fall-off of the transverse momentum distribution at the LHC energy.

The integral of the area under the fit curves carries important information about entanglement in these and other in high energy physics processes. Defining the ratio R of the integral under the power law (hard scattering component) curve, I_p and the sum of the integrals of the exponential (thermal component) curve, I_e and power law curve of the fit in **Figure 3**:

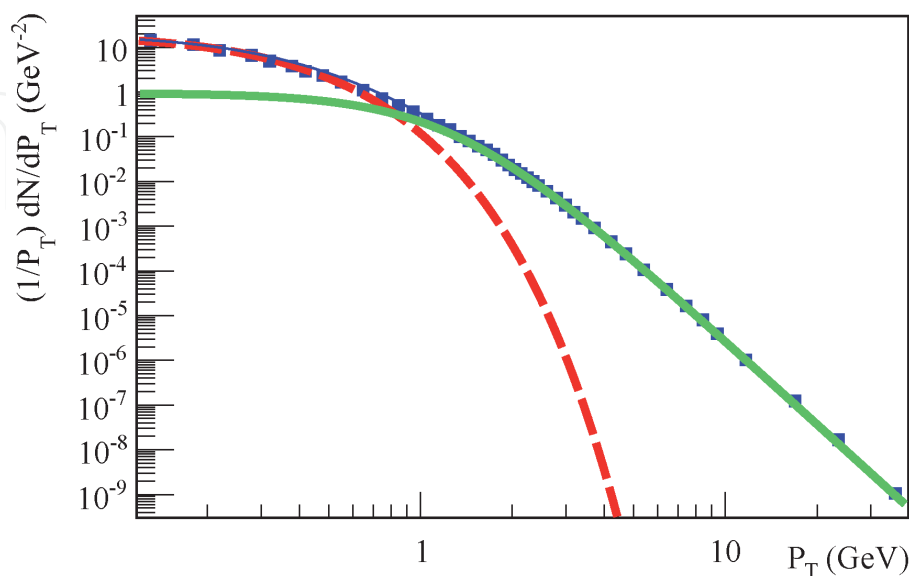


Figure 3.

Normalized transverse momentum distribution of charged hadrons from $\sqrt{s} = 13$ TeV pp collisions. The curves shown are exponential (red dashed) representing the thermal component of the distribution, and power law (green solid) corresponding to the hard scattering contribution. The superposition of these two contributions are also shown (blue, thin solid). Figure from [14], and data is from [32].

$$R = \frac{\text{power}}{\text{power} + \text{exponential}} = \frac{I_p}{I_p + I_e} \quad (10)$$

The calculation yields the value of $R \simeq 0.16 \pm 0.05$, in agreement (within the uncertainty interval) with the ratio calculated from the charged hadron spectra in inelastic proton-proton collisions at ISR energies of $\sqrt{s} = 23, 31, 45,$ and 53 GeV [20] even given the large beam energy difference between the LHC and the ISR accelerators.

2.3 Diffractive events and di-muon pair transverse momentum distribution in proton-proton collisions

Diffractive proton-proton (pp) collision events at the LHC can proceed through the photon-photon ($\gamma\gamma$) interactions shown in (Eq. (11)). Both X' and X'' can be final state protons from the collision, or the products X', X'' of their diffractive dissociation (single diffraction (in which one of the incident protons dissociates into an inelastic state), and double diffraction (in which both of the incident protons dissociate)). Measurements from the ATLAS collaboration [33] of the reaction

$$pp(\gamma\gamma) \rightarrow \mu^+ \mu^- X' X'' \quad (11)$$

at $\sqrt{s} = 13$ TeV center of mass energy in pp collisions are studied. Selection of the exclusive $\gamma\gamma \rightarrow \mu^+ \mu^-$ process was implemented by only including events that have both muon tracks (μ^+ and μ^-) while at the same time excluding events that show additional charged particle activity in the central region of the detector. Transverse momenta of greater than 400 MeV were used in the ATLAS analysis, with pseudorapidity range the same as that of the charged hadron analysis described in subSection 2.2. In the most recent ATLAS analysis of the reaction (11) only diffractive events that proceed through the $\gamma\gamma$ scattering were selected [33].

Figure 4 shows the transverse momentum distribution in the case of $\gamma\gamma$ production of di-muon pairs in pp collisions at $\sqrt{s} = 13$ TeV center of mass energy. As can

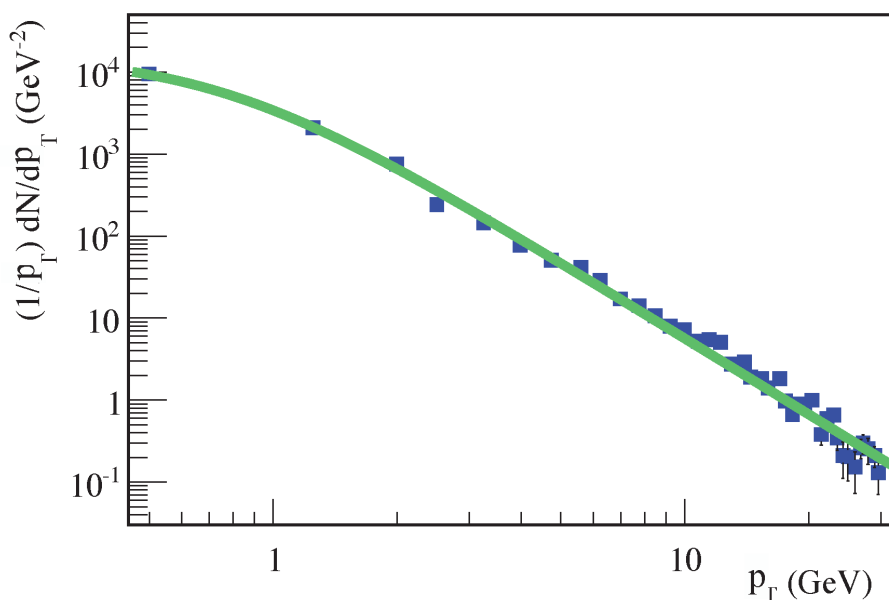


Figure 4.

The (normalized) transverse momentum diffractive scattering event distribution $\frac{1}{p_T} \frac{dN_{\mu\mu}}{dp_T}$ in units of GeV^{-2} for the reaction of (Eq. (11)) showing the absence of a thermal component to the distribution. The curve shown (green, solid) is the power law contribution corresponding to the hard-scattering process. Data from [33], figure from [14].

be seen there, the hard scattering term alone describes well the distribution, and the thermal (exponential) component is absent. As discussed already in this chapter and in [13–15], diffractive events are expected to have a suppressed thermal (exponential) component due to the fact that in these diffractive processes the photon interacts coherently with the entire proton, and no entanglement entropy is expected. This was discussed in Section 2.1. As the presence of the thermal component in this approach is the consequence of the entanglement, we expect it to be absent in diffractive events, as confirmed in **Figure 4**. Furthermore, the ratio R defined in the previous section in this case is $R \simeq 1$, in agreement with the theoretical expectations and the previous data for $\gamma\gamma$ scattering at OPAL at $\sqrt{s} = 15$ and 35 GeV that also show no thermal component. R is then equal to one within experimental uncertainty.

2.4 Combined Higgs boson decays to $\gamma\gamma$, $ZZ^* \rightarrow 4l$, and $b\bar{b}$

The Higgs boson differential transverse momentum cross section is undoubtedly adequately described by perturbation theory (see [34] for a review). An investigation is undertaken to determine whether the thermalization process due to entanglement is present in this system. The Higgs boson differential cross sections (differential in transverse momentum p_T) have been measured by both ATLAS and CMS collaborations [35–37] and most recently from [38].

In **Figure 5** the transverse momentum distribution of the Higgs bosons is shown in the range from 5 GeV to 700 GeV for combined ATLAS and CMS data at 13 TeV pp collision energy. As can be seen from **Figure 5**, there clearly are both the hard scattering (power law) and thermal (exponential) components in the transverse momentum distribution, similarly to the case explored in Section 2.2. Not surprisingly, the separation between the hard and thermal components is even more defined due to the much larger range of the available transverse momenta.

Interestingly, the ratio R defined by (Eq. (10)) and extracted from **Figure 5** is $R = 0.15 \pm 0.03$ that is very close to the one determined from the charged hadron distribution in proton-proton collisions studied in Section 2.2, $R = 0.16 \pm 0.05$.

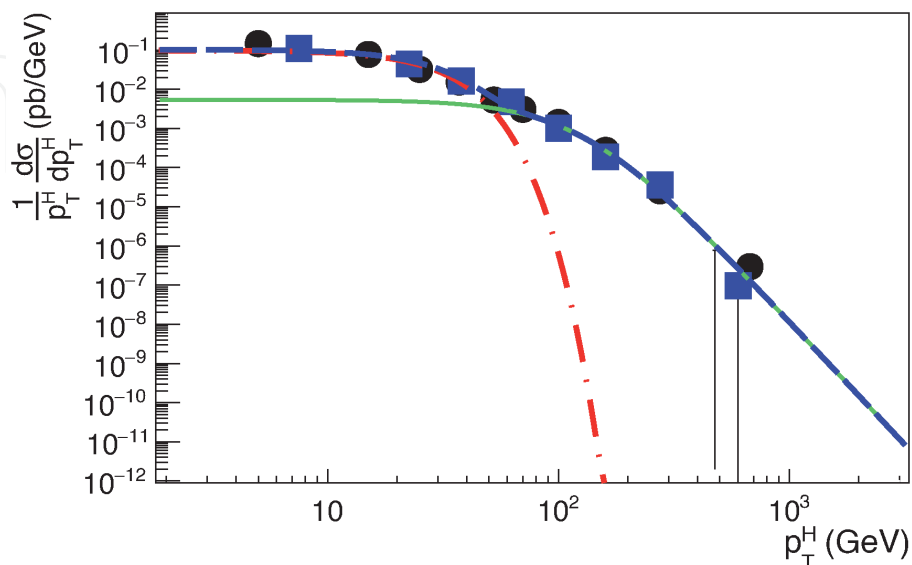


Figure 5. Normalized fiducial Higgs differential cross section versus transverse momentum reconstructed from the combination of $H \rightarrow \gamma\gamma$, four leptons, and $b\bar{b}$ decay in proton-proton collisions at $\sqrt{s} = 13$ TeV from both the ATLAS and CMS collaborations [38].

2.5 Discussion: entanglement entropy in proton-proton collisions

The material presented in Section 2 provide evidence for an unconventional mechanism of apparent thermalization in high energy pp collisions. The data shows that the effective thermal temperature T_{th} is non-universal and that it is proportional to the hard scale temperature parameter of the collision T , that is, to the momentum transfer, with $T \simeq 4.2 T_{th}$. Strikingly, this conclusion seems to apply even to the Higgs boson production, suggesting that even in this very hard process the QCD radiation may be affected by thermalization. Moreover, we have found that the thermal component of the spectrum is entirely absent in diffractive production (even though many hadrons are still produced in this case) – this again points to the non-universal, process-dependent, nature of thermalization.

The theory and the analyses of the data discussed in Section 2 appear to be consistent with the proposition that thermalization in these high energy collisions is induced by quantum entanglement. That the effective temperature determined from the data is proportional to the momentum transfer Q in the collision that provides the UV cutoff for the quantum modes, as expected. Notably, inclusive charged hadron and Higgs boson transverse momentum distributions, in which the typical momentum transfers are vastly different are in agreement in this analysis. It is seen that the thermal component is present in both cases, event though the values of the effective temperature differ by over an order of magnitude.¹

In diffractive events studied in Section 2, it is clearly seen that where studies of the coherent response of the entire proton in this scattering, there is no associated entanglement entropy [15], and that therefore there should be no thermal component to the transverse momentum distribution. The data confirms this prediction in diffractive Drell-Yan production analyzed in this section, as well as by the diffractive deep-inelastic scattering data shown in [20].

The findings presented here appear to support the proposition that a deep connection between quantum entanglement and thermalization in high-energy hadron collisions, and that this proposed link should be further investigated. Possibilities include the following as non-exhaustive examples. Combining measurements of the structure functions with the study of hadronic final states, especially in the target fragmentation region in deep inelastic scattering at the future Electron Ion Collider. Studies of the thermal component and the corresponding effective temperature in hard processes characterized by different momentum transfers in proton-proton, proton-nucleus and nucleus-nucleus collisions at RHIC and the LHC. Already, analysis of Pb–Pb HI collision data also points to a picture of thermalization as a result of quantum entanglement at high energies [9]. An investigation of the dependence of the apparent thermalization on rapidity – as depicted in **Figure 2**, suggesting that the thermal component and the corresponding effective temperature in hard processes characterized by different momentum transfer would be interesting. It suggests that thermalization is achieved faster if a measurement is performed in a smaller rapidity interval.

3. Entanglement entropy and thermal behavior in the electroweak interaction

The material and discussion in Section 2 supporting a picture of thermalization in hadronic physics due to quantum entanglement motivates an investigation of

¹ It is once again emphasized that this does not imply that the Higgs boson is produced thermally, but rather that its transverse momentum distribution is affected by thermal radiation due to entanglement.

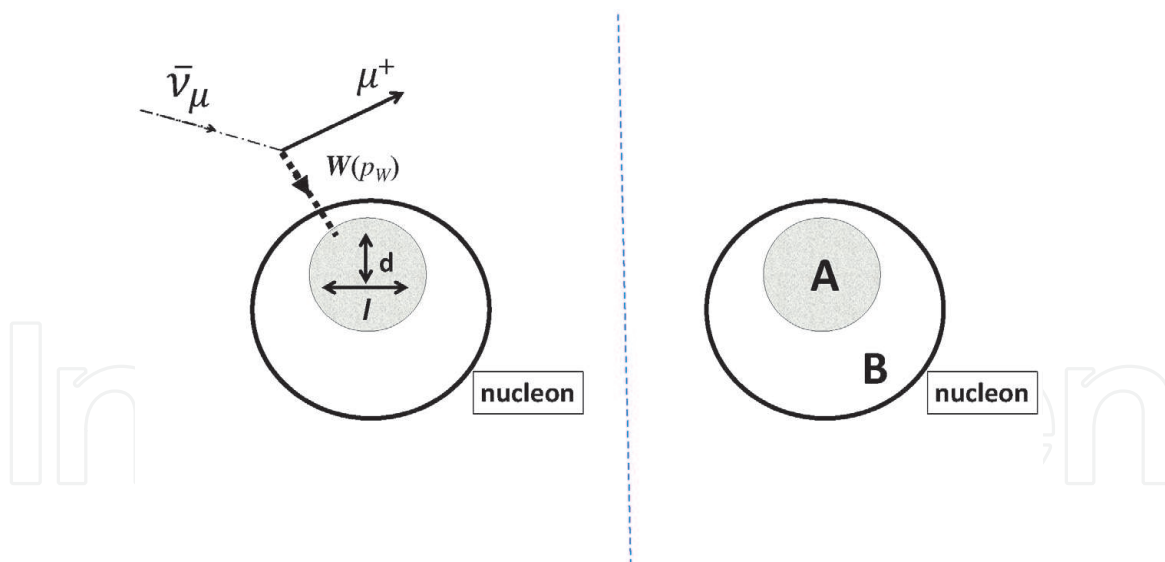


Figure 6.

(Left side) The depiction of antineutrino scattering from a nucleon via emission of a W boson with an exiting muon in the final state. The W boson samples a partial region of the nucleon, not the entire nucleon, as explained in the text. (Right side) The region of the nucleon sampled by the interacting W boson is denoted as region **A**. The nucleon spectator region not probed by the boson is region **B**. Figure from [5].

whether this same connection is manifested in weak interactions mediated by massive vector bosons. In this section that study, taken mainly from [5], is made using charged-current weak interaction processes such as

$$\bar{\nu}_\mu + N \rightarrow \mu^+ + \pi^0 + X \quad (12)$$

Similar to the partial probing of the nucleon wave function described in Section 2 the vector boson in this investigation probes only a part of the nucleon wave function, again denoted by the region **A** in **Figure 6**. This probed region has a transverse size of approximately $d = h/p_W$, and a longitudinal size of approximately $l = (mx)^{-1}$ [1, 2, 14]. In this analysis, h is Planck's constant, p_W is the boson's momentum, x is the momentum fraction carried by the struck quark in the interaction (Bjorken- x), and m is the nucleon mass. Within the struck nucleon, the probed region **A** is complementary to the spectator region **B** that is not probed in the interaction. The entire space within the nucleon (a pure state) is then **A**∪**B**. In this present analysis, as in [14], thermal behavior is attributed to the quantum entanglement between regions **A** and **B** as depicted in in **Figure 6**.

In this current analysis, we test the hypothesis, albeit disfavored by the conventional mechanism of thermalization, that the thermal feature found in the low- p_T region (corresponding to measurement at late times) of the momentum distribution can instead be attributed to the sub-nucleonic entanglement induced by collisions at high energies. This is the gist of the study using charged-current anti-neutrino interactions at the intensity frontier in particle physics. The claim from the the first two sections of this chapter is further strengthened by the demonstration that when the nucleus as a whole is scattered by the W boson so that no sub-nucleonic entanglement is produced, the thermal feature is absent from the spectrum, as expected. And that when quantum entanglement exists in the process, thermalization is present in the momentum distribution.

3.1 Charged current weak interactions: analysis and results

We begin by considering neutral pion production in charged-current antineutrino interactions with a CH (hydrocarbon scintillator) target; see (Eq. (12)). This

experimental data includes the total inclusive charged current weak interaction differential cross sections [39, 40] measurements at $1.5 \text{ GeV} < E_\nu < 10 \text{ GeV}$ [39] and data at $E_\nu = 3.6 \text{ GeV}$ [40]. The analysis results from both references, and from [5], are described in this present study. A conversion from pion kinetic energy (T_π) published in [39] to pion momentum published in [40] is made using the expression

$$\frac{d\sigma}{dp_\pi} = \frac{p_\pi c^2}{T_\pi + m_{0,\pi} c^2} \frac{d\sigma}{dT_\pi}. \quad (13)$$

The relativistic kinetic energy is related to the pion rest mass, $m_{0,\pi} c^2$, by

$$T_\pi = (\gamma - 1)m_{0,\pi} c^2 \quad (14)$$

where $\gamma = 1/\sqrt{1 - v^2/c^2}$, with v the pion velocity in this case. We will compare the above results against the inclusive charged-current coherent pion production differential cross sections given in [41].

The normalized differential cross section that is used to describe the thermal behavior from the interaction is given by a very similar formula as in subSection 2.2 but here using

$$\frac{1}{p_\pi} \frac{d\sigma}{p_\pi} = A_{\text{thermal}} e^{(-E_\pi/T_{\text{thermal}})} \quad (15)$$

where p_π ($E_\pi = \sqrt{m_\pi^2 + p_\pi^2}$) is the pion momentum (energy) and where the Mandelstam variable s is approximately equal to $m^2 + 2E_\nu m$. The hard-scattering part of the normalized momentum distribution is given by

$$\frac{1}{p_\pi} \frac{d\sigma}{p_\pi} = A_{\text{hard}} \left(1 + \frac{m_\pi^2}{T_{\text{hard}} \cdot n} \right)^{-n} \quad (16)$$

where n a power law scaling parameter. These equations are also discussed in [14, 42].

The CERN ROOT fitting program is used to fit these expressions to the MINERvA results. A total of five parameters are used in the fitting procedure: T_{thermal} , T_{hard} , n , A_{hard} , and A_{thermal} . In each case, the reduced chi-squared statistic and the fitting parameters with their associated uncertainties are recorded.

The results of fitting the thermal and hard scattering components to the distribution in the analysis using data from the MINERvA collaboration [39, 40] are shown in **Figure 7**. As can be seen from the fit, there are separate thermal (red-dashed) and hard-scattering (green-full) components in the full momentum distributions. The solid blue curve is the superposition of the exponential and power law fits.

Final state interactions (FSI) are modeled using the GENIE Monte Carlo program [43] in the analyses described in [39, 40]. They show that the larger FSI effects on the data are at low pion momenta. These effects are small compared with the statistical and other systematic uncertainties from the analysis, and did not affect the fits and conclusions drawn in this present study.

Now consider the resulting momentum distribution when the process of anti-neutrino scattering is from the entire nucleus, and not from a partial region of the nucleon as described above. That is, when the antineutrino scatters from the nucleus coherently, as in

$$\bar{\nu}_\mu + A \rightarrow \mu^+ + \pi^- + A. \quad (17)$$

In this charged current weak interaction, there is no entanglement between different parts of a struck nucleon, and no thermal component to the momentum distribution of the single produced pion is expected. It is this description of the interaction that is supported by the coherent scattering data from the MINERvA collaboration [41], as shown in **Figure 8**. Only the hard scattering (power law) fit component is needed to describe the momentum distribution. The absence of a thermal (exponential) fit component is due to the absence of entanglement in the proposition presented in this present work.

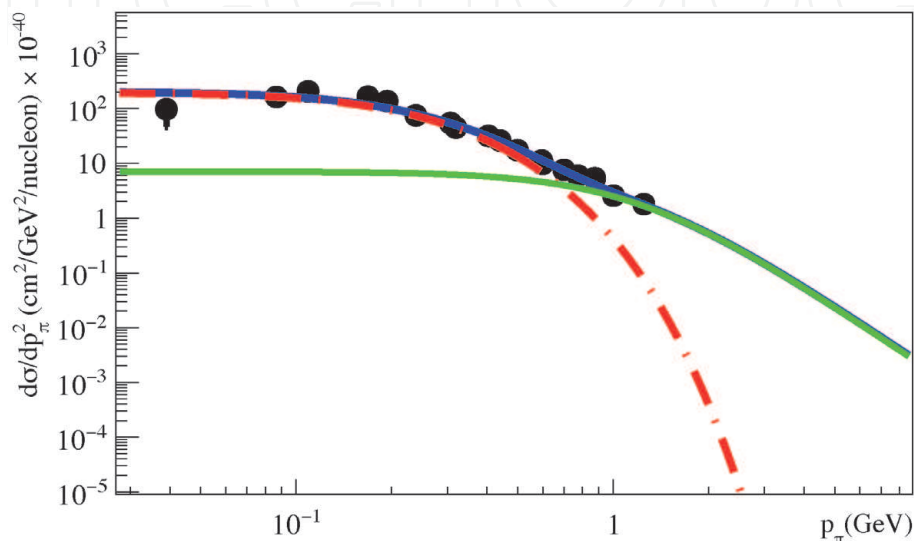


Figure 7.

Antineutrino differential cross section for scattering against hydrocarbon nuclei with resulting charged current pion production. The dashed (red) line fit to the data is the thermal component fit and the thick solid (green) line shows the hard component fit. The combined thermal and hard scattering thin solid (blue) line best fits to the data. Data taken from [39, 40]. Plot taken from [5].

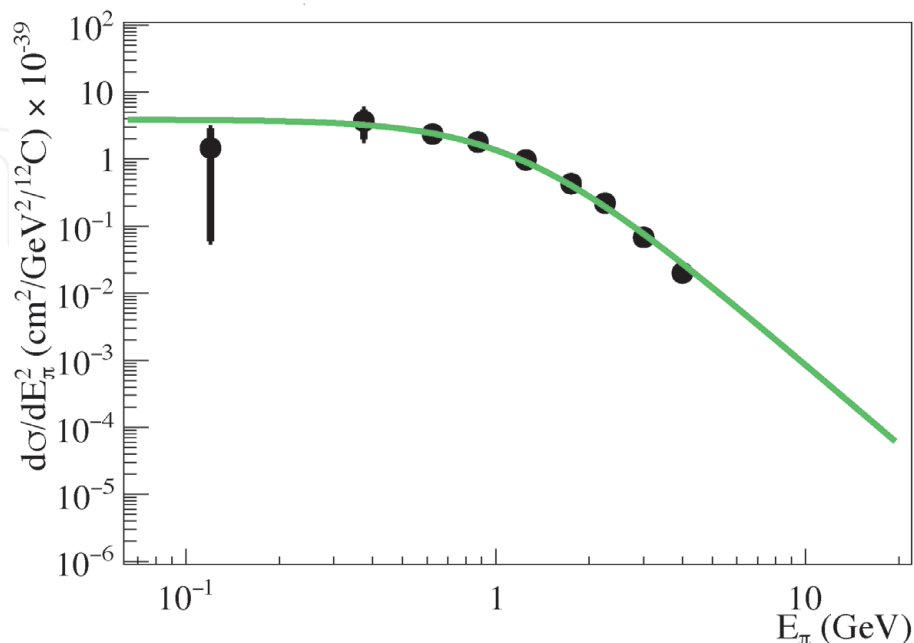


Figure 8.

Coherent scattering of the antineutrino from the hydrocarbon scintillator nuclei results in the momentum distribution shown here. The differential cross section is well described by a hard-scattering component (solid green line) alone, as expected in the absence of entanglement. The data is from [41]. The figure is from [5].

| R | Process | Reference |
|-----------------|---|-----------|
| 0.16 ± 0.05 | $pp \rightarrow$ charged hadrons | [14, 44] |
| 0.15 ± 0.05 | $pp \rightarrow H \rightarrow \gamma\gamma$ | [14, 44] |
| 0.23 ± 0.05 | $pp \rightarrow H \rightarrow 4l(e, \mu)$ | [14, 44] |
| 1.00 ± 0.02 | $pp(\gamma\gamma) \rightarrow (\mu\mu) X'X''$ | [14, 44] |
| 0.13 ± 0.03 | $\bar{\nu}_\mu + N \rightarrow \mu^+ + \pi^0 + X$ | [5] |
| 1.00 ± 0.05 | $\bar{\nu}_\mu + {}^{12}\text{C} \rightarrow \mu^+ + \pi^- + {}^{12}\text{C}$ | [5] |

Table 1. The ratio R is defined in (Eq. (10)) for different processes as shown. The results listed indicate that the thermal behavior due to entanglement entropy is independent of the interaction (strong or electroweak) but process dependent.

4. Conclusion

R (Eq. (10)) is computed from the integral of the combined fit, which combines the hard-scattering function (Eq. (16)) and the exponential function (Eq. (15)). The R values obtained in charged-current weak interactions are consistent with values obtained for pp collisions [14]. And as stated in Section 2 they are also in agreement (within experimental uncertainty) with values obtained from low energy ISR and HERA data [20]. **Table 1** presents a compilation of the ratio R (defined by (10)) for the processes considered in this present study.

The results presented in this study support those given in [1, 2, 14, 18], namely that quantum entanglement in hadrons is what gives rise to the thermal behavior observed in hadronic collisions and, as the new results from charged-current neutrino scattering presented here suggest, that the thermalization process from entanglement, while process dependent, is interaction independent.

Author details

Oliver Keith Baker
 Department of Physics, Yale University, New Haven, CT, USA

*Address all correspondence to: oliver.baker@yale.edu

IntechOpen

© 2021 The Author(s). Licensee IntechOpen. This chapter is distributed under the terms of the Creative Commons Attribution License (<http://creativecommons.org/licenses/by/3.0/>), which permits unrestricted use, distribution, and reproduction in any medium, provided the original work is properly cited. 

References

- [1] D. E. Kharzeev, E. M. Levin, Deep inelastic scattering as a probe of entanglement, *Phys. Rev. D* **95** (11) (2017) 114008.
- [2] A. A. Bylinkin, D. E. Kharzeev, A. A. Rostovtsev, The origin of thermal component in the transverse momentum spectra in high energy hadronic processes, *Int. J. Mod. Phys. E* **23** (12) (2014) 1450083.
- [3] , R. Hagedorn, Statistical thermodynamics of strong interactions at high energies, *Nuovo Cim. Suppl.* **3**, 147 (1965); Hadronic matter near the boiling point, *Nuovo Cim. A*, **56**, 1027 (1965).
- [4] , F. Becattini, An introduction to the Statistical Hadronization Model, arXiv: 0901.3643 [hep-ph] (2009).
- [5] G. Iskander, J. Pan, M. Tyler, C. Weber, O.K. Baker, Quantum Entanglement and Thermal Behavior in Charged-Current Weak Interactions, *Phys Lett B* **811**, 135948 (2020).
- [6] G. Ramos, M. Machado, Investigating entanglement entropy at small- x in dis off protons and nuclei, *Phys. Rev. D* **101** (2020) 074040.
- [7] M. Mezei, W. van der Schee, Black holes often saturate entanglement entropy the fastest, *Phys. Rev. Lett.* **124** (2020) 201601–201606.
- [8] T. T. Takahashi, Y. Kanada-En'yo, Lattice QCD study of static quark and antiquark correlations via entanglement entropies, *Phys. Rev. D* **100** (2019) 114502.
- [9] X. Feal, C. Pajares, R. A. Vazquez, Thermal behavior and entanglement in Pb-Pb and pp collisions, *Phys. Rev. C* **99** (1) (2019) 015205.
- [10] C. M. Ho, S. D. H. Hsu, Entanglement and fast quantum thermalization in heavy ion collisions, *Mod. Phys. Lett. A* **31** (18) (2016) 1650110.
- [11] P. Castorina, A. Iorio, D. Lanteri, P. Lukes, Gluon shadowing and nuclear entanglement, arXiv:2003.00112v1 [hep-ph] (Feb. 2020).
- [12] S. Beane, P. Ehlers, Chiral symmetry breaking, entanglement, and the nucleon spin decomposition, Report Number NT@UW-19-06; arXiv: 1905.03295v1 [hep-ph] (May 2019).
- [13] A.A. Bylinkin, D.E. Kharzeev, and A.A. Rostovtsev, “The origin of thermal component in the transverse momentum spectra in high energy hadronic processes”, *Physics Preprint Archives arXiv:1407.4087*, 1 (2014).
- [14] O. K. Baker, D. E. Kharzeev, Thermal radiation and entanglement in proton-proton collisions at the LHC, *Phys. Rev. D* **98** (5) (2018) 054007.
- [15] , D.E. Kharzeev, and E.M.Levin, “Deep inelastic scattering as a probe of entanglement” *Phys Rev D* **95**, Number 11, 114008 (2017).
- [16] A.M. Kaufman, M.E. Tai, A. Lukin, M. Rispoli, R. Schittko, P.M. Preiss, M. Greiner, “Quantum thermalization through entanglement in an isolated many-body system”, *Science* **353**, Number 6301, 794-800 (2016).
- [17] P. Calabrese and J. Cardy, “Evolution of entanglement entropy in one-dimensional systems”, *Journal of Statistical Mechanics: Theory and Experiment* **2005**, Number 04, P04010 (2005).
- [18] P. Calabrese and J. Cardy, “Quantum quenches in 1+1 dimensional conformal

- field theories”, *Journal of Statistical Mechanics: Theory and Experiment* **2016**, Number 06, 064003 (2016).
- [19] P. Calabrese and J. Cardy, “Quantum quenches in extended systems”, *Journal of Statistical Mechanics: Theory and Experiment* **2007**, Number 06, P06008 (2007).
- [20] A.A. Bylinkin and A.A. Rostovtsev, “Role of quarks in hadroproduction in high energy collisions”, *Physics Preprint Archives arXiv:1404.7302*, 1 (2014).
- [21] P. Jurcevic et al. *Nature* **511**, 7508, 202 (2014).
- [22] M. Rigol, V. Dunjko, V. Yurovsky, and M. Olshanii *Phys. Rev. Lett.*, **98**(5), 050405 (2007).
- [23] Z. X. Gong, L.M. Duan, *New Journal of Physics*, **15**(11), 113051 (2013).
- [24] D.E Kharzeev and K. Tuchin, “From color glass condensate to quark–gluon plasma through the event horizon”, *Nucl. Phys.* **A753** Number 3-4, 316 (2005).
- [25] G. Dunne and T. Hall, “QED effective action in time dependent electric backgrounds”, *Phys. Rev.* **D58**, Number 10, 105022 (1998).
- [26] P. Castorina, D. Kharzeev and H. Satz, *Eur. Phys. J. C* **52**, 187 (2007).
- [27] D.E. Kharzeev, E. Levin, and K. Tuchin, “Multiparticle production and thermalization in high-energy QCD”, *Phys. Rev.* **C75**, Number 4, 044903 (2007).
- [28] R. Baier, A. H. Mueller, D. Schiff and D. T. Son, *Phys. Lett. B* **502**, 51 (2001) doi:10.1016/S0370-2693(01)00191-5 [hep-ph/0009237].
- [29] S. Lin and E. Shuryak, *Phys. Rev. D* **77**, 085013 (2008) doi:10.1103/PhysRevD.77.085013 [hep-ph/0610168].
- [30] V. Balasubramanian *et al.*, *Phys. Rev. D* **84**, 026010 (2011) doi:10.1103/PhysRevD.84.026010 [arXiv:1103.2683 [hep-th] (2011)].
- [31] J. Berges, S. Floerchinger and R. Venugopalan, arXiv:1707.05338 [hep-ph] (2017).
- [32] The ATLAS collaboration, “Charged-particle distributions at low transverse momentum in $\sqrt{s} = 13$ TeV pp interactions measured with the ATLAS detector at the LHC”, *Eur. Phys. J.* **C76**, 502 (2016); The ATLAS collaboration, Charged-particle distributions in $\sqrt{s} = 13$ TeV pp interactions measured with the ATLAS detector at the LHC’, *Phys Lett.* **B758**, 67 (2016).
- [33] The ATLAS collaboration, Measurement of the exclusive $\gamma\gamma \rightarrow \mu\mu$ process in proton-proton collisions at $\sqrt{s} = 13$ TeV with the ATLAS detector, *Phys. Lett.* **B777**, 303 (2018); arXiv: 1708.04053 (2017).
- [34] S. Dittmaier *et al.* [LHC Higgs Cross Section Working Group], doi:10.5170/CERN-2011-002 arXiv:1101.0593 [hep-ph] (2011).
- [35] The ATLAS collaboration, “Measurement of inclusive and differential cross sections in the $H \rightarrow 4l$ decay channel in pp collisions at $\sqrt{s} = 13$ TeV with the ATLAS detector”, *J. High Energ. Phys.*, 2017: 132 (2017).
- [36] Eleni Mountricha on behalf of the ATLAS collaboration, “Higgs Measurements in High Resolution Channels with ATLAS”, LHCP2017, Large Hadron Collider Physics Conference, Shanghai, China, June 2017 (2017).

[37] J. Tao on behalf of the CMS collaboration, “Higgs boson measurements in high resolution channels with CMS”, Physics Preprint Archives arXiv:1708.09215, 1 (2017).

[38] ATLAS and CMS collaborations, European Physical Society Conference on High Energy Physics (EPS-HEP) , July 10-17 (2019), <https://indico.cern.ch/event/577856/> (2019).

[39] C. L. McGivern, et al., “Cross sections for neutrino and antineutrino induced pion production on hydrocarbon in the few-GeV region using MINERvA,” Phys. Rev. D 94, 052005 (2016).

[40] T. Le, et al., “Single neutral pion production by charged-current ν_μ interactions on hydrocarbon at $\langle E_\nu \rangle = 3.6$ GeV”, Phys. Lett. B 749, 130 (2015).

[41] A. Mislivec, et al., “Measurement of total and differential cross sections of neutrino and antineutrino coherent π production on carbon”, Phys. Rev. D 97, 032014 (2018).

[42] A. Bylinkin, A. Rostovtsev, “Role of quarks in hadroproduction in high energy collisions”, Nucl. Phys. B 888, 65 (2014).

[43] C. Andreopoulos, et al., “The GENIE Neutrino Monte Carlo Generator”, Nucl. Instrum. Meth. 614 (2010) 87–104.

[44] C. Weber, O. K. Baker, D. Kharzeev, “Quantum Entanglement and Proton- Proton Collisions at the LHC”, SUSY International Conference, Corpus Christie, TX (2019) (Jul. 2019).